Chinese Chemical Letters 31 (2020) 1644–1647

Contents lists available at ScienceDirect

Chinese Chemical Letters

journal homepage: www.elsevier.com/locate/cclet

Communication

Peony pollen derived nitrogen-doped activated carbon for supercapacitor application

Yiming Liu[a], Zhongxun An[b], Mingxia Wu[b], Anbao Yuan[a], Hongbin Zhao[a,*], Jiujun Zhang[a], Jiaqiang Xu[a,*]

[a] NEST Lab, Department of Physics, Department of Chemistry, College of Sciences, Shanghai University, Shanghai 200444, China
[b] National Engineering Research Center for Supercapacitor for Vechicles, Shanghai AOWEI Technology Development Co., Ltd., Shanghai 201203, China

ARTICLE INFO

Article history:
Received 28 June 2019
Received in revised form 22 July 2019
Accepted 5 August 2019
Available online 6 August 2019

Keywords:
Supercapacitors
Biomass
Nitrogen-doped
Hierarchical carbon
Peony pollen

ABSTRACT

Peony pollen is a cheap and readily available biomass material with a relatively high protein content. In this work, it was employed as an N-rich precursor to prepare the nitrogen-doped porous carbon for supercapacitor application. The porous carbon microspheres were prepared through a hydrothermal method and subsequent carbonization process. Notably, ammonium borofruoride and potassium hydroxide were employed respectively as an etchant and an activator to modify the porosity of the materials. The as prepared ANPPCs-700 has a super high BET specific surface area of 824.69 m^2/g. The microstructure, chemical state and electrochemical properties of the product were investigated in detail. The prepared nitrogen-doped carbon microspheres exhibits excellent specific capacity of 209 F/g at a current density of 1A/g and remained 92.5% of the initial capacitance after 5000 deep cycles at 5A/g.

The depletion of fossil energy and increasing environmental issue has forced human society to seek renewable energy sources as well as high efficiency power storage systems. In recent years, supercapacitors have attracted unparalleled attention, it offers bright future to electric energy storage and transportation owning to its first-rate charge/discharge speed, superior cycle stability and relatively high energy density [1]. According to different electronic storage mechanisms, supercapacitors can be segregated into two categories, *i.e.,* electrical double layer capacitors (EDLC) and pseudocapacitors. During the past 50 years, carbon materials are repeatedly researched and widely used in EDLC because of their good conductivity, environmental adaptability, structure stability and low cost. However, traditional carbon materials like activated carbon has limited specific capacitance as a result of their low specific surface area as well as lack of electrochemically active site [2]. Several excellent reviews indicated that nitrogen doping in carbon materials is an effective way to enhance electrochemical performance and increase the pseudocapacitance of supercapacitors [3,4]. It has been proved that the existence of pyridinic N, pyrrolic N and graphitic N in carbon materials can promote the electrochemical performance of the supercapacitors [5,6], which accelerate the electronic conductivity and increase the ions of electrolyte to load on the surface of the electrode material due to its large ionic binding energy. In addition, nitrogen-containing group can also provide the ionic active site of the material during the charge/discharge process, enhancing the pesudocapacitance and wettability [7,8].

Much work so far has focused on synthesizing nitrogen-doped carbon materials. For example, nitrogen-containing polymers like polyaniline [9,10], pyrrole [11] and polyacrylonitrile [12] are often employed as precursors to synthesize nitrogen-doped carbon materials. However, these precursor preparation processes are cumbersome, and have adverse effects on the environment. Biomass materials are eye-catching in recent years due to their sustainability and environmental friendliness [13]. A wide variety of biomass materials were carbonized and then utilized as supercapacitor materials, such as bamboo [14], rose [15], prawn shells [16], silkworm [17].

Similar to other biomass materials, peony pollen is widely available in nature and has a high protein content, meaning more nitrogen content [18]. Classified by morphology, pollen can be divided into single groove pollen, three groove pollen, three-hole pollen and multi-hole according to its surface structure. Peony pollen belongs to multi-hole pollen, its porous outer surface makes it easy to react with other chemicals and modify the morphology through the pretreatment process. Recent research indicates that employ NH_4BF_4 as an etchant can make high specific surface area

* Corresponding authors.
E-mail addresses: hongbinzhao@shu.edu.cn (H. Zhao), xujiaqiang@shu.edu.cn (J. Xu).

https://doi.org/10.1016/j.cclet.2019.08.005
1001-8417/

porous carbon [19]. The introduction of fluoride atoms leads to the formation of fluorocarbon bonds, after treatment with high temperature, the fluorocarbon bonds decomposed and broke the internal structure of the material. The particle size of the prepared carbon material can be controlled by adjusting the carbonization temperature of the material.

Material synthesis is divided into hydrothermal reaction and calcination. First, the peony pollen was reacted with ammonium borofruoride to form a fluorocarbon bond by a hydrothermal method. Then the product was carbonized in a tube furnace at 700 °C for 2 h to decompose the fluorocarbon bonds. The obtained carbon materials were further activated by using potassium hydroxide. The obtained ANPPCs (activated nitrogen doped peony pollen carbon sphere) show an ultra-high specific capacitance (209 F/g) at 1 A/g current density as well as a durable cycle life for 92.5% capacity retention rate after 5000 deep cycles.

Fig. 1 exhibits scanning electron microscopy (SEM) and mapping images of ANPPCs-700. Fig. 1a shows the as synthesized materials consisting of spherical carbon in different sizes, roughly 1–3 μm in diameter. It can be inferred that during the hydrothermal process, the pollen shells are broken into small pieces while the internal components of the pollen spontaneously assembled by dehydration and sintering into carbon spheres. And in the wake of the carbonization process, the carbon spheres retain their original microstructure. Figs. S1b and c (Supporting information) display the SEM of NPPCs-600 and NPPCs-800. As the carbonization temperature increases, the original shape gradually shattered and turned into fragmented pollen shells and carbon microspheres. Moreover, it can be seen from Fig. 1b that the ANPPCs-700 activated by KOH have an uneven surface comparing with NPPCs-700 (Fig. S1d in Supporting information). This might be caused by the reaction of KOH with carbon, and subsequent release of gases such as carbon monoxide and hydrogen, further generating pores inside and outside the material. As a comparison, ANPPC-700

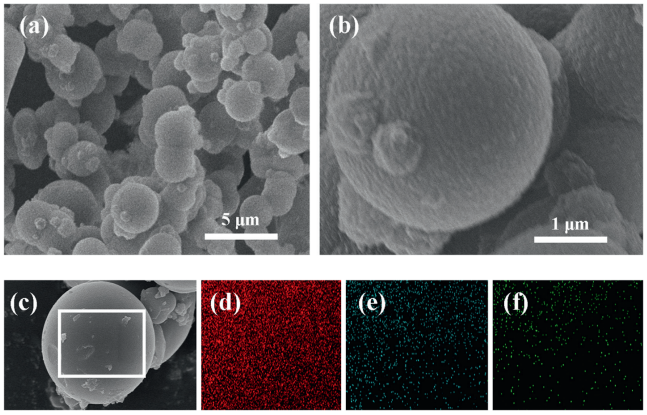

Fig. 1. (a) SEM image of ANPPCs-700; (b) Enlarged image of ANPPCs-700; (c–f) SEM image of ANPPCs-700 and the elements mapping corresponding to C (d), N (e), O (f).

(Fig. S1a in Supporting information) activated directly by KOH is a relatively amorphous porous carbon with uneven size. Figs. 1c-f show the elemental mapping of ANPPCs-700, revealing that C, O, N are uniformly distributed in ANPPCs-700 and the proportion of N composition is 1.43%.

The X-ray powder diffraction patterns are displayed in Fig. 2a, all the samples reveal two broad peaks at ~24° and ~43°, corresponding to an amorphous state of carbon. Three sharp peaks observed at 28.2°, 40.6° and 47.1° are presumably characteristic peaks of the $(CF_{1.1})_n$. The (002) crystal planes of graphite and fluorocarbon are shifted to a small angle, indicating that the doping of F atoms is a replacement of C atoms, forming a semi-ionic fluorocarbon bond [19]. However, through KOH activation process biomass carbon appreciably decline in intensity and moves to a small angle, speculating that inside change of the material is a

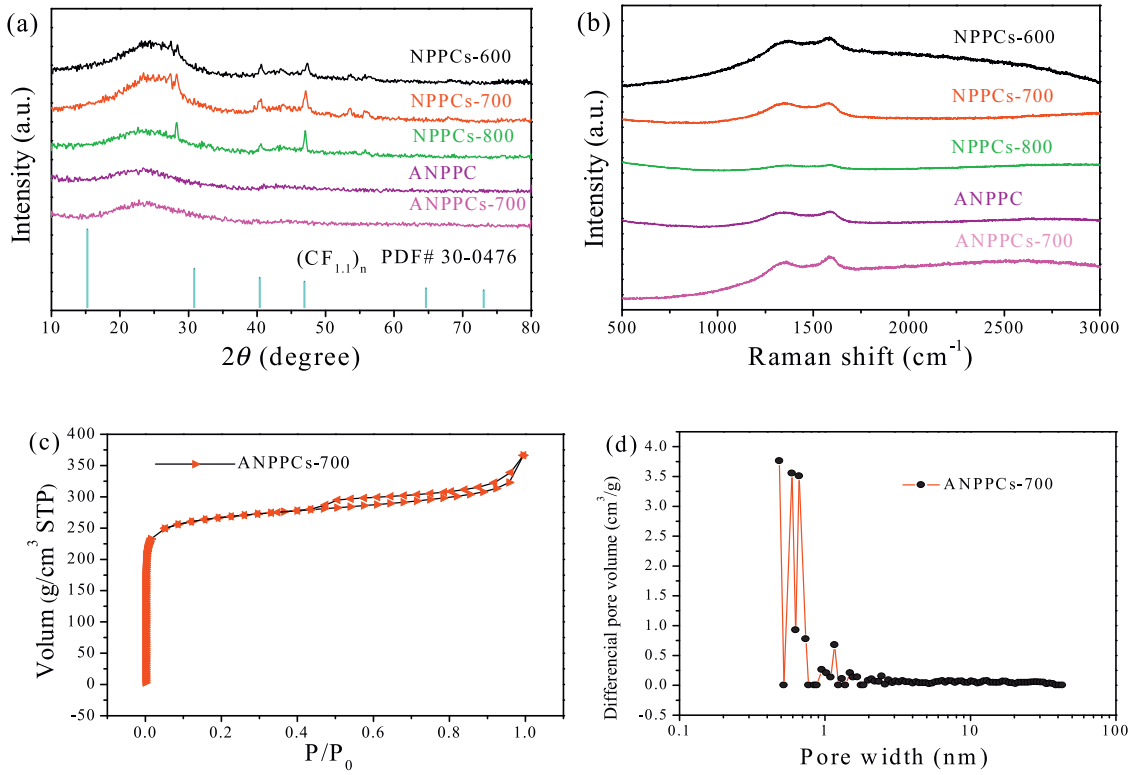

Fig. 2. (a) XRD patterns and crystal structure analysis of the as-prepared materials; (b) Raman spectra of the as-prepared materials; (c) Nitrogen adsorption/desorption isotherms and (d) the pore size distribution curves of ANPPCs-700.

messy accumulation of carbon atoms and reduction of graphitization carbon [20]. Moreover, the fluorocarbon peak disappeared, revealing that F leaves the material as fluorocarbon after activation. Raman spectroscopy was conducted as well to further investigate the structure of the carbon spheres. It can be inferred from Fig. 2b that all the samples have two bands at ~1349 cm^{-1} and ~1590 cm^{-1}. These two bands are considered to be disordered defects (D band) and ordered sp^2 graphitic plane (G band) of carbon [21]. The I_D/I_G ratio of NPPCs-600, NPPCs-700, NPPCs-800, ANPPC-700 and ANPPCs-700 are 0.98, 0.99, 0.99, 0.98 and 0.88, respectively. The intensity of the D and G bands gradually decreases along with the carbonization temperature raised, which is consistent with the observation from XRD. However, there is no significant change of I_D/I_G ratio as temperature altering. In addition, the ratio of I_D/I_G is reduced again when KOH is applied for the material activation, suggesting a higher degree of graphitization of the samples [22].

Pore properties of the materials were determined by nitrogen adsorption-desorption at 77 K. As shown in Fig. 2c, sample ANPPCs-700 shows the combination of type I and type IV isotherms, suggesting the filling phenomenon in mesoporous material. In the meanwhile, a hysteresis loop of H4 type appears when the P/P_0 value is around 0.4, further indicating the existence of mesopores and crack pores [23]. The BET specific surface area of the material is 824.69 m^2/g and the adsorption average pore diameter is around 2.75 nm. The pore size distribution is shown in Fig. 2d, micropores less than 2 nm occupies the highest proportion of the ANPPCs-700, and a large amount of mesopores were distributed in the range of 2–40 nm, which can be seen from the enlarged image (Fig. S2 in Supporting information).

The X-ray photoelectron spectroscopy (XPS) analysis was carried out to further study the elemental content and chemical state of the nitrogen group in the materials (Fig. 3). The full XPS spectra of the samples are shown in Fig. 3a, peaks located in 285, 400 and 532 eV are corresponding with C 1s, N 1s and O 1s, respectively. In addition, NPPC-700 shows the peak of F 1s at 685 eV while others did not perform, which is consistent with the observation of XRD. Fig. S3 (Supporting information) shows high-resolution C 1s XPS spectrum of ANPPCs-700, which can be separated into three peaks at 284.5 eV, 285 eV and 289 eV, corresponding to C=C, C–N and O-C=O. N 1s high-resolution spectra of NPPC-700, ANPPCs-700 and ANPPC-700 (Figs. 3b-d) could be further separated into three different peaks at the binding energies of 398.1, 399.3 and 400.5 eV, attributing to pyridinic N, pyrrolic N and graphitic N groups, respectively. It is worth noting that graphitic N of the ANPPCs-700 is significantly reduced compared with the NPPCs-700 before activation. The FT-IR spectroscopies (Fig. S4 in Supporting information) of NPPC-700, ANPPCs-700 and ANPPC display wide peaks at ~1100 cm^{-1}, also suggesting the existence of C–N bonds and C–O groups [24].

The electrochemical measurements of NPPCs-600, NPPCs-700, NPPCs-800, ANPPCs -700 and ANPPC were conducted to further explore the effects of carbonization temperature and KOH activation on the electrochemical performance of the as-prepared materials. The CV (cyclic voltammetry) curves of all the samples were tested by using a three-electrode system in 6 mol/L KOH electrolyte with a potential window of −1 V to 0 V (*vs.* Hg/HgO). As can be seen in Fig. 4a, the CV curve of each sample basically maintains a consistent quasi-rectangular shape, which can be described as a standard electric double layer capacitance. It is significant that a slight redox peak appears at the voltage of 0.41 V, indicating that the materials may have a certain pseudocapacitance. Graphite carbon defect sites associated with nitrogen doping can be converted into electrochemically active species to increase the redox capacity of the material without affecting conductivity [25].The results show that 700 °C is the most suitable carbonization temperature, the as-prepared material possesses the highest specific capacitance and ANPPCs-700 obviously has a higher specific capacitance over others. This is nearly identical to the results of galvanostatic charge/discharge curves in Fig. S5 (Supporting information). According to previous studies, the major contribution of the pseudocapacitance comes from pyridinic N and pyrrolic N [26]. Optimistically, the introduction of KOH activation not only coordinated both porosity and graphitic N group content of ANPPCs-700 but also retained pyridinic N and pyrrolic N content [27].

Fig. 4b shows the CV curves of the ANPPCs-700 at different scan rates from 10 mV/s to 100 mV/s. It can be seen that the similar quasi-rectangular shape is maintained, suggesting the exceptional rate capability of the ANPPCs-700 [23]. GCD curves of ANPPCs-700 at different current density in Fig. 4c indicates a nearly isosceles triangle, further illustrating the electric double layer capacitance characteristics of the ANPPCs-700. The specific capacities of the ANPPCs-700 are 225, 209, 186, 136 and 130 F/g at current densities of 0.5, 1, 2, 5 and 10 A/g, displayed a capacity retention of 62.22% (Fig. S6 in Supporting information). This is mainly because the porous structure enables fast ion diffusion and nitrogen doping provide active reaction sites. Subsequently, the long cycle test (Fig. S7 in Supporting information) was performed in 6 mol/L KOH at 5 A/g current density, the ANPPCs-700 electrode exhibits splendid long-term cycling stability of 92.5% capacity retention after 5000 deep cycles. This is mainly owning to the hierarchical porosity and structure stability of ANPPCs-700.

Electrochemical impedance spectrum was employed to further study AC impedance behavior of the samples. As is shown in Fig. 4d, in high-frequency region, the intersection value of the semicircle and the real axis represent the internal resistance (R_s) of the electrode active material and the electrolyte. It can be observed from the AC impedance spectrum that both ANPPCs-700 (0.59 Ω) and NPPCs-700 (0.42 Ω) have low R_s. This can be assigned to the result of nitrogen doping, which increased the conductivity and wettability of the material. From the mediate frequency region, the smaller charge-transfer resistance (R_{ct}) of ANPPCs-700 than NPPCs-700 may be attributed to the formation of interconnected micropores and mesopores during KOH activation process. The hierarchical pore structure provides channels for the transport of ions [28]. In low-frequency region, the plot of ANPPCs-700 is more vertical than

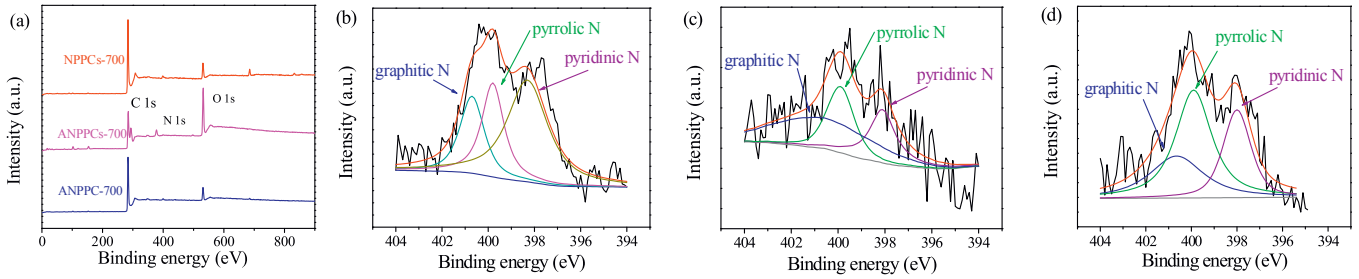

Fig. 3. (a) The XPS survey scan of NPPCs-700, ANPPCs-700 and ANPPC-700; High-resolution N 1s XPS spectra of (b) NPPC-700, (c) ANPPCs-700, (d) ANPPC-700.

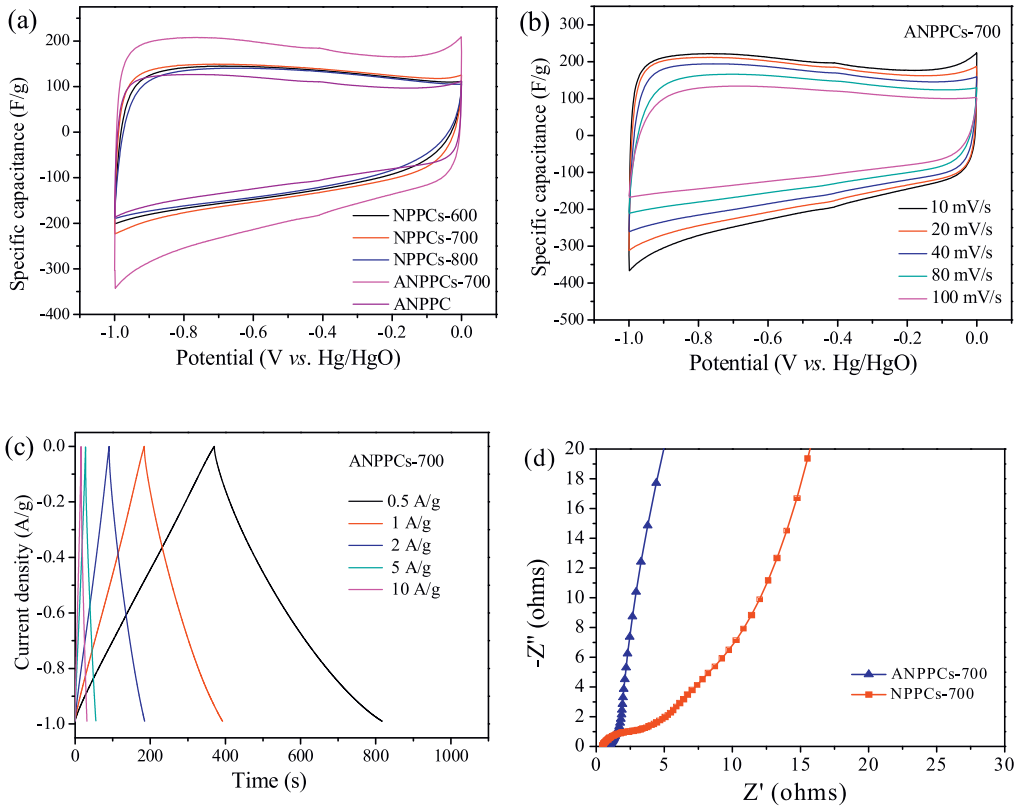

Fig. 4. (a) The CV curves of NPPCs-600, NPPCs-700, NPPCs-800, ANPPCs-700 and ANPPC-700; (b) The CV curves of ANPPCs-700 at different scan rates; (c) The galvanostatic charge-discharge curve of ANPPCs-700 at diff ;erent specific current density; (d) Nyquist plots of ANPPCs-700.

that of NPPCs-700, suggesting the typical capacitor characteristics [29]. Meanwhile, the EIS of NPPCs-700 is a typical "Randles" electric circuit that was controlled by diffusion process from electrolyte to electrode materials and the 45° slop line represent the Warbug resistance (Z_w) section.

Over all, by introducing hydrothermal reaction with NH_4BF_4 and high temperature treatment, the biomass carbon material can be crushed to a certain size of carbon microspheres and the size can be controlled by changing the temperature. The obtained nitrogen doping carbon microspheres has a certain pseudocapacitance. Furthermore, the KOH activation process forms miropores and mesopores inside the materials that increases the specific surface of the material, thereby improving the electric double layer capacitance. The prepared ANPPCs-700 has a good specific capacitance of 209 F/g as well as an excellent cycle stability, retaining 92.5% of its initial capacity after 5000 cycles.

Acknowledgment

We gratefully acknowledge financial supports from the National Key Research and Development Program of China (Nos. 2017YFB0102200, 2017YFB0102900).

Appendix A. Supplementary data

Supplementary material related to this article can be found, in the online version, at doi:https://doi.org/10.1016/j.cclet.2019.08.005.

References

[1] W. Raza, F. Ali, N. Raza, et al., Nano Energy 52 (2018) 441–473.
[2] B. Li, F. Dai, Q.F. Xiao, et al., Energy Environ.Sci. 9 (2016) 102–106.
[3] S. Herou, P. Schlee, A.B. Jorge, et al., Curr. Opin. Green Sustain. Chem. 9 (2018) 18–24.
[4] G. Wang, L. Zhang, J. Zhang. Chem. Soc. Rev. 41 (2012) 797–828.
[5] G.X. Lin, R.G. Ma, Y. Zhou, et al., Electrochimi. Acta 261 (2018) 49–57.
[6] Z. Min, P. Fan, W. Zhao, et al., Carbon 68 (2014) 185–194.
[7] X.J. Wei, Sg. Wan, S.Y. Gao, Nano Energy 28 (2016) 206–215.
[8] J.Y. Zhu, X. Dan, C.C. Wang, et al., Carbon 115 (2017) 1–10.
[9] S.K. Kandasamy, K. Kandasamy, J. Inorg. Organomet. Polym. Mater. 28 (2018) 559–584.
[10] Y. Meng, K. Wang, Y. Zhang, et al., Adv. Mater. 25 (2013) 6985–6990.
[11] J.B. Zhu, T.Y. Feng, X.F. Du, et al., J. Power Sources 346 (2017) 120–127.
[12] Y. Long, G.Z. Yang, H. Pan, et al., J. Power Sources 315 (2016) 209–217.
[13] Y.Q. Zhang, X. Liu, S.L. Wang, et al., Adv. Energy Mater. 7 (2017) 1700592.
[14] G.X. Zhang, Y.M. Chen, Y.G. Chen, et al., Mater. Res. Bull. 102 (2018) 391–398.
[15] C.J. Zhao, Y.X. Huang, C.H. Zhao, et al., Electrochimi. Acta 291 (2018) 287–296.
[16] F. Gao, J.Y. Qu, Z.B. Zhao, et al., Electrochimi. Acta 190 (2016) 1134–1141.
[17] S.J. Lei, L.F. Chen, Z. Wei, et al., J. Power Sources 379 (2018) 74–83.
[18] Y. Tao, L.Y. Wang, J. Beijing Forestry Univ. 24 (2002) 5–11.
[19] J.S. Zhou, J. Lian, L. Hou, et al., Nat. Commun. 6 (2015) 8590.
[20] M. Swvilla, A.B. Fuertes, Carbon 56 (2013) 155–166.
[21] Y.H. Zhao, M.X. Liu, X.X. Deng, et al., Electrochimi. Acta 153 (2015) 448–455.
[22] J.N. Yi, Q. Yan, C.T. Wu, et al., J. Power Sources 351 (2017) 130–137.
[23] M.X. Liu, L.H. Gan, X. Wei, et al., Energ. Fuel. 27 (2013) 1168–1173.
[24] Z.Y. Lin, G. Waller, L. Yan, et al., Adv. Energy Mater. 2 (2012) 884–888.
[25] T.Q. Lin, I.W. Chen, F.X. Liu, et al., Science 350 (2015) 1508-1503.
[26] D. Hulicovajurcakova, Adv. Funct. Mater. 19 (2010) 1800–1809.
[27] G. Ma, Q. Yang, K. Sun, et al., Bioresour. Technol. 197 (2015) 137–142.
[28] J.Q. Zhou, M. Wang, X. Li, J. Porous Mat. 26 (2019) 99–108.
[29] H.K. Song, Y.H. Jung, K.H. Lee, et al., Electrochimi. Acta 44 (1999) 3513–3519.